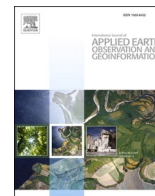




Contents lists available at ScienceDirect

International Journal of Applied Earth Observation and Geoinformation

journal homepage: www.elsevier.com/locate/jag

Dynamic rainfall-induced landslide susceptibility: A step towards a unified forecasting system

Mahnoor Ahmed^{a,*}, Hakan Tanyas^b, Raphaël Huser^c, Ashok Dahal^b, Giacomo Titti^d,
Lisa Borgatti^d, Mirko Francioni^a, Luigi Lombardo^b

^a Department of Pure and Applied Sciences, University of Urbino 'Carlo Bo', Campus Scientifico Enrico Mattei, Via Cà le Suore, 2/4, 61029 Urbino, Italy

^b University of Twente, Faculty of Geo-Information Science and Earth Observation (ITC), PO Box 217, Enschede, AE 7500, Netherlands

^c Statistics Program, Computer, Electrical and Mathematical Sciences and Engineering (CEMSE) Division, King Abdullah University of Science and Technology (KAUST), Thuwal 23955-6900, Saudi Arabia

^d Department of Civil Chemical Environmental and Materials Engineering, Alma Mater Studiorum University of Bologna, Bologna, Italy

ARTICLE INFO

Keywords:

Dynamic susceptibility
Landslide prediction
Early warning system
Generalized additive models

ABSTRACT

The initial inception of the landslide susceptibility concept defined it as a static property of the landscape, explaining the proneness of certain locations to generate slope failures. Since the spread of data-driven probabilistic solutions though, the original susceptibility definition has been challenged to incorporate dynamic elements that would lead the occurrence probability to change both in space and in time. This is the starting point of this work, which combines the traditional strengths of the susceptibility framework together with the strengths typical of landslide early warning systems. Specifically, we model landslide occurrences in the norther sector of Vietnam, using a multi-temporal landslide inventory recently released by NASA. A set of static (terrain) and dynamic (cumulated rainfall) covariates are selected to explain the landslide presence/absence distribution via a Bayesian version of a binomial Generalized Additive Models (GAM). Thanks to the large spatiotemporal domain under consideration, we include a large suite of cross-validation routines, testing the landslide prediction through random sampling, as well as through stratified spatial and temporal sampling. We even extend the model test towards regions far away from the study site, to be used as external validation datasets. The overall performance appears to be quite high, with Area Under the Curve (AUC) values in the range of excellent model results, and very few localized exceptions.

This model structure may serve as the basis for a new generation of early warning systems. However, the use of The Climate Hazards group Infrared Precipitation with Stations (CHIRPS) for the rainfall component limits the model ability in terms of future prediction. Therefore, we envision subsequent development to take this direction and move towards a unified dynamic landslide forecast. Ultimately, as a proof-of-concept, we have also implemented a potential early warning system in Google Earth Engine.

1. Introduction

The need to understand landslide dynamics comes from the disastrous impacts, with average economic losses recorded up to 5 billion USD for susceptible countries such as Japan, United States and India (Hidayat et al., 2019). Aside from the financial aspects, Petley (2012) reported over 32,000 victims globally in the years 2004–2010. With an increase in the frequency of rainfall extremes, the impacts are also expected to worsen over time (Hidayat et al., 2019). To limit the impact due to landslides, Early Warning Systems (EWS) are commonly

implemented to assist in management and precautionary measurements on regional levels (Guzzetti et al., 2020; Naidu et al., 2018). Particularly for rainfall-induced landslides (RIL), an early warning system is typically developed by setting a rainfall-threshold that, once exceeded, initiates the system to issue alarms for further measures (Guzzetti et al., 2008; Segoni et al., 2018). These systems can be developed over large regions as well as at the scale of single landslides (Guzzetti et al., 2020). In the first case, rainfall data is usually accessed from national rain gauge networks (Al-Thwaynee et al., 2023), or even from satellite data (Wang et al., 2021) to estimate potentially unstable areas and their

* Corresponding author.

E-mail address: m.ahmed4@campus.uniurb.it (M. Ahmed).

<https://doi.org/10.1016/j.jag.2023.103593>

Received 1 August 2023; Received in revised form 23 November 2023; Accepted 26 November 2023

Available online 3 December 2023

1569-8432/© 2023 The Author(s). Published by Elsevier B.V. This is an open access article under the CC BY license (<http://creativecommons.org/licenses/by/4.0/>).

temporal aspect. As for localized early warnings, they can usually rely on a rich hydrological and geotechnical information gathered through landslide-specific installations, from which rainfall thresholds are still derived to understand possible slope failures timing (Segoni et al., 2018). Aside from the scale at which these tools are developed and used, another level of differentiation comes from the underlying methods they may rely on the definition of suitable thresholds. Specifically, both physically and statistically-based approaches constitute valid solutions (Guzzetti et al., 2020). Physics-based models essentially use detailed slope information in terms of its morphological structure, lithological characteristics and hydrological conditions to quantify the rainfall amount needed to trigger a failure (Guzzetti et al., 2007). Conversely, data-driven approaches (Chauhan et al., 2010; Guzzetti et al., 2020; He et al., 2021) do not deterministically solve hydro-mechanical equations but rather rely on historical landslide inventories to probabilistically estimate rainfall intensity-duration relations (Guzzetti et al., 2007). These relations are the foundation for the definition of rainfall thresholds in a given area. As for the concept of intensity-duration, this revolves around combining precipitation amounts in a given period of time, whose length determines the required accumulation for failure to initiate (Guzzetti et al., 2020). Nowadays, most of the methods belonging to the latter class follow a quite standard procedure where alert levels are defined purely on the basis of rainfall estimates. This is considered independently from the proneness or susceptibility to failure typical of a given landscape. However, the orographic effect influences rainfall patterns, especially in highlands (Adler et al., 2003; Gariano et al., 2017; Guzzetti et al., 2008; Kirschbaum et al., 2012; Nguyen et al., 2014). This element only comes in a second stage, with static susceptibility maps being combined only with a geographic overlay criterion (Lee et al., 2008). This post-processing routine contributes to the hazard level assigned to a given spatial unit (Kirschbaum and Stanley, 2018). Decoupling the landscape response into its two main components may have been a suitable solution in the past, due to the limited computational tools. However, nowadays modeling approaches increasingly offer the ability to combine landslide susceptibility and rainfall thresholds in a single platform, with an inspirational example by Steger et al. (2023). Moreover, the reliability of EWS significantly changes across the globe, with regions that are able to rely on dense rain gauge networks as compared to those that lack resources and are limited in their data acquisition. In the case of Vietnam the spatial scale at which Landslide Early Warning Systems (LEWS) are developed varies significantly. There exists a number of such systems that require in-situ soil data as well as equipment operated and maintained by manual labor at catchment or slope level (Bui et al., 2013, 2012, 2011; Gian et al., 2017; Ha et al., 2020). In-field measurements are of a more accurate nature and may be temporally consistent. However, they offer discrete spatial information and are infeasible to acquire over a larger extent. For this reason, we can recently witness an increasing use of alternative rainfall information estimated from radar satellites (Hong et al., 2006; Kirschbaum et al., 2012, 2009).

For extending the geographic scale, satellite products can offer very good temporal data, though generally at the expense of the spatial resolution (Tang et al., 2020). Moreover, the availability of near-real-time satellite products allowed the evaluation of potential landslide hazard prediction, initially by using the Tropical Rainfall Measuring Mission (TRMM) Multi-satellite Precipitation Analysis (TMPA) at a relatively large spatial scale (Hong et al., 2006; Hong and Adler, 2007). Advancing on the basis of integrating satellite information, Hong & Adler (2007) later proposed an EWS based on real-time precipitation systems, tested on global and regional scales by Kirschbaum et al. (2012). Building on these steps, the most recent development on a global scale using the diversity of satellite products is the release of Landslide Hazard Assessment for Situational Awareness (LHASA) by NASA which provides moderate to high landslide hazard every half hour (Kirschbaum and Stanley, 2018). With the second version of LHASA in place (Stanley et al., 2021), the core of the model relies on a static susceptibility map

overlaid with dynamic rainfall forecasts to produce landslide predictions globally in real time, with new components added for increasing predictive power. However, a two-phased model such as LHASA essentially neglects the natural interaction of rainfall with terrain for modelling rainfall-induced landslides. Moreover, its current version does not account for uncertainty estimation, which should be particularly important to connect the uncertainty coming from the static susceptibility component to the dynamic precipitation component.

In this work, we combine the static and dynamic effects responsible for landslide occurrences in north Vietnam using a single space-time model. Specifically, we used a Bayesian approach to account for uncertainties and framed it in a Binomial GAM. Statistical influence was performed using the Integrated Nested Laplace Approximation (INLA; Rue et al., 2009) method, which provides fast computation of posteriori quantities of interest.

2. Study area and materials

The following section provides an insight into the event-based landslide inventory used in this work and the selection of the complementary study area. Moreover, it describes the mapping unit used and covariate information used as an input to our model and the validation techniques implemented.

2.1. Study area and landslide inventory information

Among the vulnerable southeast-Asian countries (Titti et al., 2021), Vietnam shows the highest number of fatalities due to landslides in the rainy season extending from June to November (Amatya et al., 2022). For this reason, NASA's efforts produced a landslide inventory for the Lower Mekong Region (LMR) for multiple rainfall triggering events (see Fig. 1). The resulting multi-temporal landslide inventory was generated using a semi-automated mapping approach (Amatya et al., 2022), that we also used to test LHASA at a regional scale (Biswas et al., 2022). These inventories are six and seem to reflect some degree of clustering although, this is mostly due to the space-time mapping approach that NASA followed.

For the present experiment, we only extracted landslides that occurred within north-western Vietnam and use that as our study area shown in Fig. 1. This landslide subset accounts for a total of 9,310 landslides, clustered into 6 rainfall triggered events, as listed in Table 1.

This area is over 59,000 km² wide with a mountainous topography and it also represents the poorest sector in Vietnam (Bangalore et al., 2019). Therefore, the impact of landslide occurrences tends to have even worse impacts.

2.2. Mapping unit

Due to the spatial extent of the study area and to also ensure the use of a suitable mapping unit, we opted to partition the study area into Slope Units (SUs; Carrara et al., 1991). This spatial partition is rooted in the landslide literature and has offered a valid alternative to grid-cells (Reichenbach et al., 2018). The reason for their success lies in their ability to reflect the morpho-dynamic response of a slope if a landslide triggers at that specific location. In other words, these mapping units can be considered independent of each other (or very weakly dependent) for landslide susceptibility purposes (Lombardo et al., 2020; Titti et al., 2021). To delineate such slope unit partition, we used the *r.slopeunits* tool proposed by Alvioli et al. (2016). This tool can be called from GRASS GIS (Neteler and Mitasova, 2013) and only requires a Digital Elevation Model (DEM) as the input. Here we used the Shuttle Radar Topography Mission (SRTM; Yang et al., 2011). As for how *r.slopeunits* works, it essentially clusters grids with analogous slope exposition and vectorize the results for a given study site. This is achieved by constraining the procedure through a set of parameters whose explanation can be found in Alvioli et al. (2016). For this work, we initially tested a

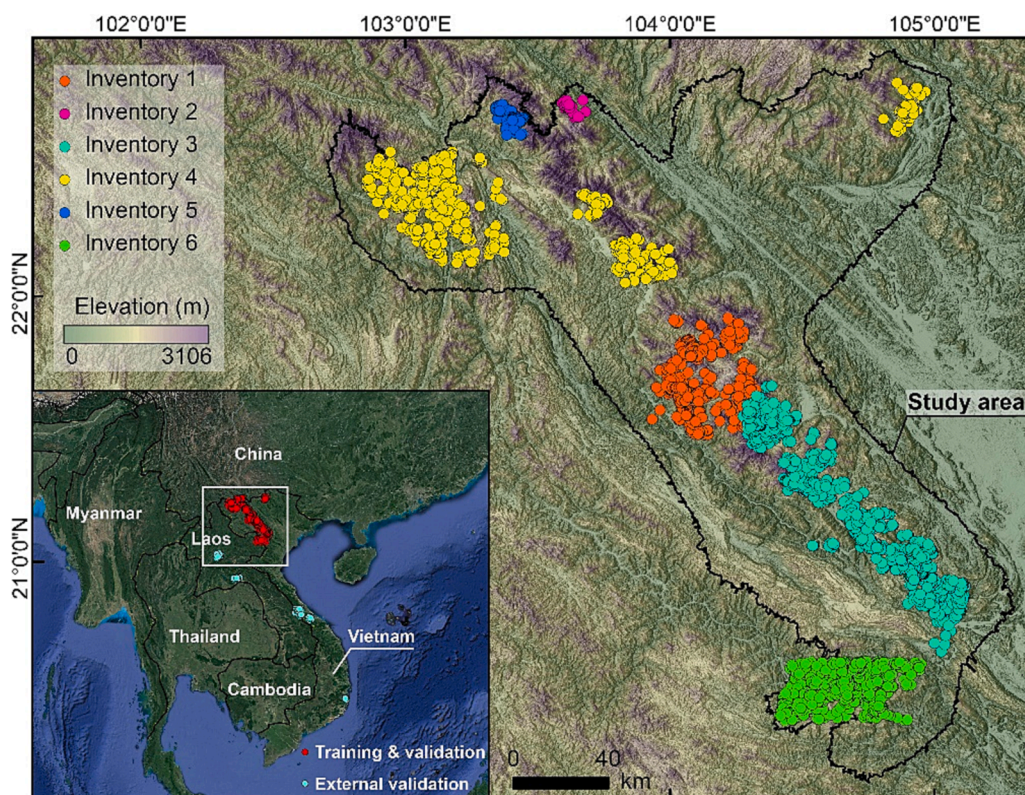


Fig. 1. Landslide points mapped by NASA in the Lower Mekong Region (Amatya et al., 2022) and the study area defined in North-western Vietnam. The lower-left panel reports the administrative boundaries in black solid lines, and the corresponding countries are labelled in white.

Table 1

Details of the multi-temporal landslide inventory contained in the study area (Fig. 1), generated by Amatya et al. (2022).

Year	Inventory	Date	Landslide Points
2017	1	2nd-3rd August	2014
	2	23rd-28th August	99
	3	10th-11th October	3944
2018	4	23rd-24th June	1310
	5	3rd August	302
	6	27th August-1st September	1641

number of possible parameter combinations (unreported results) and opted for a final setting as shown in Table 2.

2.3. Predictors

2.3.1. Dynamic covariates

An important aspect of this study is the estimation of rainfall effect in landslide events that can be used to project future landslide susceptibility scenarios using a predictive equation. Prolonged rainfall before the landslide event contributes towards slope saturation (Guzzetti et al., 2008; Segoni et al., 2018), which was integrated to develop cumulative antecedent rainfall (Chikalamo et al., 2020). This represents the dual

Table 2

Parameter setting for generating slope units in the study area using r. slopunits.

Parameter	Set Value
Minimum area of SU	40000 m ²
Circular variance	0.5
Large flow accumulation threshold	800,000 m ²
Clean size	20,000 m ²
Number of iterations	20

rainfall effect (the event day and potential recent discharge prior to the event) as the triggering factor. To represent the spatio-temporal distribution of precipitation for each event, together with cumulative antecedent rainfall, we used CHIRPS (Funk et al., 2015). This choice is mainly due to the relatively high spatial resolution (~5.5 km) of this global product. As for its temporal characteristics, CHIRPS offers daily rainfall aggregates achieved with a 2-day latency (Funk et al., 2015).

Alongside to the rainfall characteristics, we also considered including dynamic vegetation indices as part of our covariate set. We therefore opted for using Enhanced Vegetation Index (EVI) obtained from MODIS AQUA (Didan, 2015) at approximately 250 m of spatial resolution and a 16-day revisit time. Notably, both products were accessed, preprocessed and downloaded through Google Earth Engine (GEE; Gorelick et al., 2017; Mutanga and Kumar, 2019). There we aggregated them at the SU scale by taking the maximum daily rainfall as well as the mean 16-day value of the EVI.

2.3.2. Static covariates

Static predictors were also extracted through GEE. Specifically, we accessed the cloud-available SRTM DEM at 30 m resolution and computed terrain attributes by using the SRT function built by Titti et al. (2022). This tool allows to compute terrain characteristics and aggregate them at any spatial scale. The latter is a particularly important requirement because of the SU partition we opted for. In fact, hundreds of DEM pixels can fall in a single SU and therefore summary statistics of the corresponding covariate distribution per polygon have to be computed. Here we do so by taking the mean and standard deviation of every continuous covariate. These have been selected among a number of standard landslide predisposing factors in the susceptibility literature (see Budimir et al., 2015), listed as follows: (1) Elevation (Görüm, 2019), (2) Slope steepness (Wu and Sidle, 1995), (3) Planar and (4) Profile curvatures (Ohlmacher, 2007), (5) Eastness (Leempoel et al., 2015), (6) Northness (Epifanio et al., 2014) and (7) Internal Relief (Görüm, 2019;

Qiu et al., 2018).

3. Method

3.1. Modeling framework

To model landslide susceptibility in space and time, we used a Bayesian version of a binomial GAM (Hastie, 2017). Assuming a priori that the probability of landslide occurrence can only be explained through a linear function may not hold for all predictors one may choose. For this reason, a GAM is much more versatile as it allows for the integration of linear as well as non-linear effects (Goetz et al., 2015). A logistic GAM, expressed for binary data (namely landslide presence/absence), can be formulated in its simplest form through its equation for the log-odds as follows;

$$\log p/1-p = \beta_0 + \beta_1\chi_1 + \dots + \beta_m\chi_m + f(\chi_{m+1}) \quad (1)$$

where P indicates the probability of landslide presence in a mapping unit, β_0 is the global intercept, each β_i represents the regression coefficient of the accompanying covariate (χ_i), which are assumed to have a linear effect on unstable slope units and f expresses nonlinear function of the covariate χ_{m+1} . In practice, non-linear effects may be implemented by discretizing the continuous covariate χ_{m+1} into n discrete classes and enforcing statistical dependence (e.g., through an autoregressive structure) between the effects of neighboring classes.

The modelling process has been implemented using R-INLA (Integrated Nested Laplace Approximation) package of R (RStudio Team, 2023), commonly used for support Bayesian inference (Rue et al., 2009).

3.2. Antecedent rainfall-window

Intensity-duration relationships (Guzzetti et al., 2007, 2006; Hong et al., 2006; Kirschbaum et al., 2012) have been an essential part in most of the traditional LEWS. To adhere to that concept as part of our space-time modeling approach, we also explored the effect of cumulative antecedent rainfall. We do so by computing rainfall as 14 potential aggregated covariates, corresponding to the maximum daily sums from the day of the triggering event (inclusive) to the 14th day before the landslide occurrence. Specifically, we fit 14 separate space-time susceptibility models and then use the Watanabe Akaike Information Criteria (WAIC; Whalen and Hoppitt, 2016) to select the most suitable day representing the intensity-duration effect. WAIC is commonly used as a model selection tool, which can be used to compare sets of covariates in order to identify the ideal combination whilst keeping the rest of the parameters the same. In fact, model ranking can be obtained by sorting WAIC in ascending order since the lowest value represents the best predictor set. Notably, Amatya et al. (2022) could not assign a specific landslide triggering day to each inventory out of the six we consider here. Therefore, not only the WAIC is here used to indicate the most suitable antecedent window but also the best triggering day, within the error date reported by the authors.

3.3. Validation techniques

Any susceptibility model needs to be equipped with a validation phase necessary to evaluate its capacity to suitably predict an unknown dataset (Chung and Fabbri, 2008, 2003; Lombardo and Tanyas, 2020; Remondo et al., 2003). Most of the landslide community adopts a purely random approach for validation (Neuhäuser et al., 2012). However, such bootstrap techniques do not usually perturb the dataset to the point of disaggregating the spatial structure in the data (Brenning, 2005). Thus, the resulting performances do not stray away from the ones estimated for the fit. This is why a fewer number of more rigorous articles adopt a spatial-cross-validation (SCV) technique instead (see Brenning, 2012). For space-time models, the context explained above is even more

relevant. In fact, removing observations entirely at random from a large spatio-temporal domain, leaves most of the data structure unchanged. Therefore, the resulting performances may be misleadingly and almost as high as for the fit to the entire observed dataset. For this reason, it is important to design suitable cross-validation (CV) techniques, and combine the SCV framework shown in Lin et al. (2021) together with temporal CV routines. In this work, we tested a number of those to retrieve the full spectrum of modeling performance offered by our space-time susceptibility model; more details will be provided below. For all of them, we will use the AUC of the Receiver Operator Characteristic (ROC) curve, as a performance indicator (Yang and Berdine, 2017; Zou et al., 2007).

3.3.1. Unstructured cross-validation

The simplest validation routine we adopt is a 10-fold CV for which we partition the space-time domain into ten mutually-exclusive subsets for training (90 %) and testing (10 %).

3.3.2. Spatial cross-validation

Here we create a large gridded lattice (Fig. 2), which we iteratively use to select all the single-grid-intersected slope units for validation. The complementary sample, is used instead for calibration.

3.3.3. Temporal cross-validation

Here we opted for a dual temporal CV approach. The first one boils down to a leave-one-landslide-event-out (LOLEO) routine, where five out of six inventories are used for calibration and the predictive performance are iteratively monitored over the excluded inventory.

By contrast, the second approach uses a sequential criterion where the first model is built using only the first inventory (in time) and is validated over the second. In the next step, the model integrates the first and second inventories validating over the third, until the last test uses the sixth inventory for validation, being trained over the combination of all the previous ones.

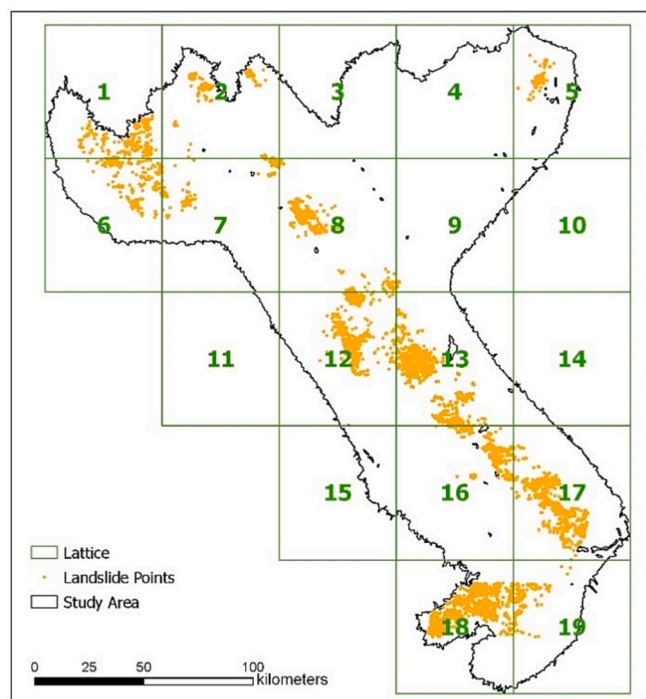


Fig. 2. Representation of the lattice over the study area for spatial validation scheme.

3.3.4. External cross-validation

Even in the case of the validation suites we described above, the locations and time used for testing are essentially the same as used for the model fit. We opted to include another validation step based on an independent dataset to check if our model is able to extrapolate to a different space–time domain. We recall here that the multi-temporal landslide inventory mapped by NASA covers the LMR (see [Amatya et al., 2022](#)). We therefore decided to use three landslide clusters in Vietnam and two from Laos (shown later in [Fig. 8](#)) as the prediction target.

4. Results

4.1. Antecedent rainfall-window

To select the best fitting cumulative rainfall capable to explain the landslide distribution, we computed the precipitation aggregated over multiple antecedent windows and retrieved the corresponding WAIC of each model. In complementary manner, for each aggregated rainfall measure, we also computed a LOLEO-CV to assist the selection of a suitable rainfall window. Both WAIC and AUC values are shown in [Table 3](#), where we sorted the cumulative antecedent rainfall windows with ascending WAIC values. Interestingly, the WAIC and AUC seem to point out at slightly different antecedent windows. If we look at the WAIC results, the best antecedent rainfall corresponds to the 2-days cumulative antecedent rainfall window. Conversely, the highest average AUC across LOLEO-CVs belongs to 8-days antecedent rainfall window. An interesting consideration to be made here is, despite the fact that we tested up to 14 days of antecedent rain, the top half of the ranked performance table only includes a maximum of 9 antecedent days. This may indicate that any long-term meteorological signal may not bring any additional information to the model. In other words, it is the short-term rainfall discharge that controls the landslide distribution in the study area.

As for the most suitable specific rainfall window, the first two best models according to the WAIC correspond to 1-day and 2-days prior to the landslide event. We recall that in [Section 2.1](#), the maximum dating error among landslide-events was up to 6 days. For this reason, a WAIC-oriented choice would lead to a time window contained within the potential dating error. Hence, looking at the next viable option, the 8-days antecedent precipitation ranks third with the lowest WAIC, but also corresponds to the highest AUC resulted from the LOLEO-CV. For this reason, we opted for the 8-days' time-window in the remainder of the manuscript, to be used as our reference antecedent window for rainfall during the modeling phase.

4.2. Model fit

In this section, we initially present the estimated covariate effects, both in their linear and nonlinear forms (see [Fig. 3](#)). Specifically, out of the sixteen covariates used for this study, mean Slope (expressed in degrees), Internal Relief (expressed in meters) and Maximum Distance (also expressed in meters) were modelled as ordinal variables, with an adjacent-class-dependence driven by a Random Walk of first order

Table 3

First 7 models sorted in ascending order of WAIC with corresponding ROC-AUC values of the temporal validation.

Antecedent Rainfall Days	WAIC	Average AUC
2	23492.17	0.828
1	23636.73	0.827
8	23685.13	0.831
3	23735.00	0.830
9	23790.42	0.818
4	23824.17	0.829
7	23834.70	0.830

(RW1; for more information see [Bakka et al., 2018](#)). The remaining covariates were all featured as linear effects in the model ([Fig. 3a](#)). This choice emerged from a number of unreported test where we individually checked each covariate behavior, to isolate those that clearly required a non-linear use.

In [Fig. 3c](#), the mean slope displays an increasing trend, demonstrating the overall positive effect of the slope steepness to instability. A detailed look highlights a marked negative contribution until approximately 25°. From this point, the mean slope regression coefficient becomes increasingly positive up to 35° after which it flattens out. The posterior distribution of the mean relief ([Fig. 3b](#)) also varies in its effect. It starts by depicting a positive trend until ~ 600 m, after which the curve indicates a decrease towards negligible effects from around 1200 m onwards. The use of the SU maximum distance is meant to convey shape characteristics into the model under the assumption that elongated slope units may be more suitable for the development of shallow flow-like landslides such as the ones that comprise the inventory. This is reflected in the marginal plot ([Fig. 3d](#)), where short distances are associated to negative regression coefficients, which rapidly become positive already at maximum lengths of 2000 m.

As for the contribution brought by the linear effects, significantly positive contributing covariates include elevation (standard deviation), Eastness (mean), planar curvature (standard deviation), Northness (mean and standard deviation), antecedent rainfall and EVI (standard deviation). Conversely, significantly negative contributions correspond to elevation (mean), slope (standard deviation), profile curvature (mean and standard deviation), EVI (mean) and roundness index of the slope unit.

We present here the model results in map form by plotting summary statistics out of each susceptibility map. Specifically, our space–time model returns the full posterior distribution of the susceptibility, from which we initially estimate two metrics namely, the posterior mean and width of the 95 % credible interval (CI), measured as the difference between the 97.5 and 2.5 percentiles of the susceptibility for each of the six landslide events. These results are later combined by showing in [Fig. 4](#), the mean value of the six posterior mean susceptibility distributions across the six maps ([Fig. 4a](#)), together with the mean of the posterior 95 % CI measured across the same ([Fig. 4b](#)).

4.3. Unstructured cross-validation

Sampling the spatio-temporal domain into 10 random subsets and validating each subset yields an excellent model performance. [Fig. 5](#) displays the individual output of each validated subset. The relative range of the AUC for the ROC curves is shown as the boxplot in [Fig. 5](#), which ranges between 0.855 and 0.880.

4.4. Spatial cross-validation

The grid numbers of the lattice over the study area ([Fig. 2](#)) are used as validation blocks with their representative performances summarised in [Fig. 6](#). The corresponding AUC values show a variation within the grid-cells containing uneven SUs (study area covered). However, only a few blocks result in $0.6 < \text{AUC} < 0.7$, while the rest reports good to excellent values.

4.5. Temporal cross-validation

In this section, we present two different temporal validation routines. We recall that the first one makes use of the first inventory to predict the second, then a combination of the first two to predict the third and so on until the sixth one. Conversely, the second routine (LOLEO) calibrates over five inventories and predicts the sixth one, for each inventory separately. [Fig. 7a](#) summarises the sequential validation performance of our model, which appears to produce good classification results according to [Hosmer et al. \(2003\)](#). Differently from the previous

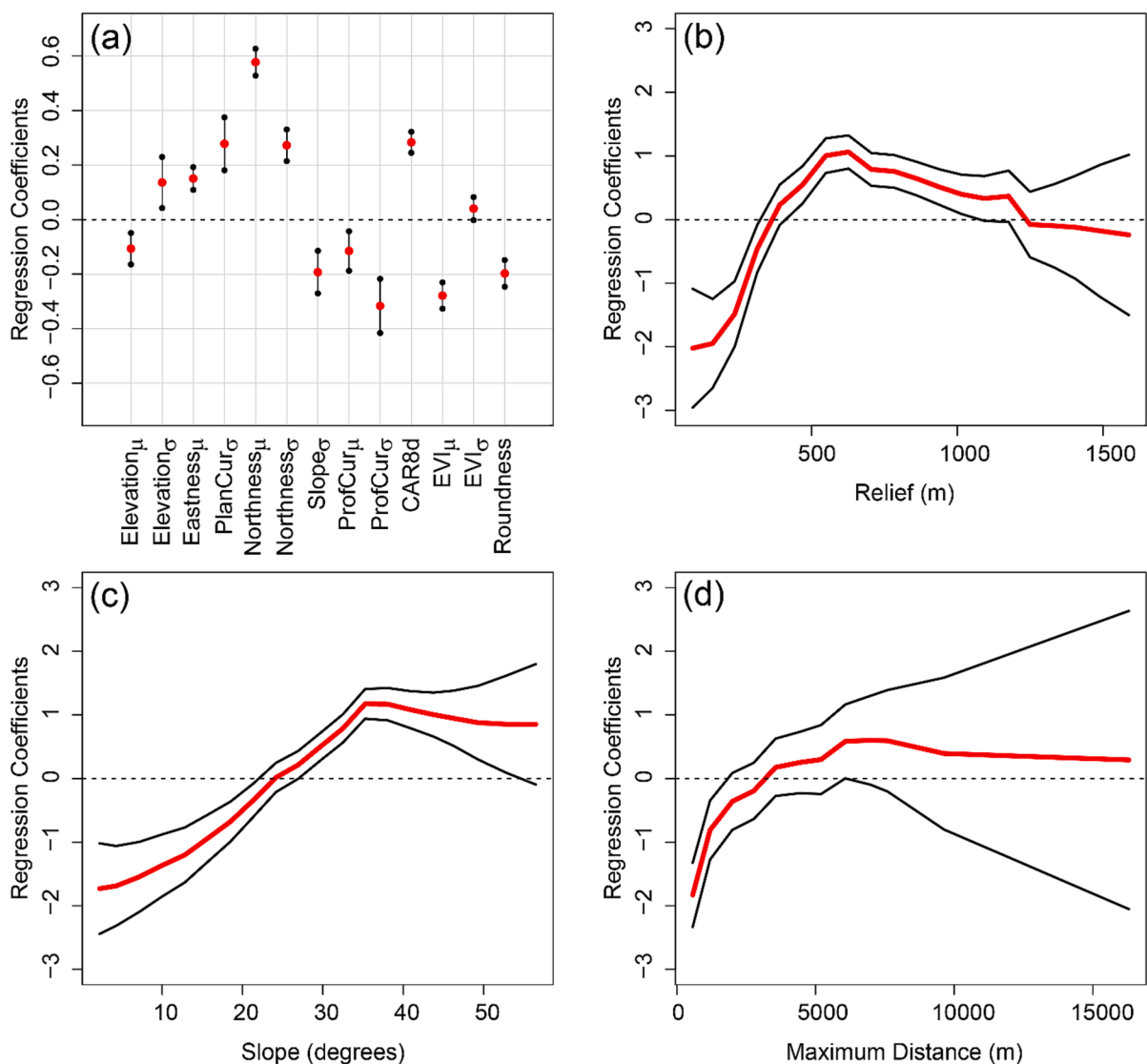


Fig. 3. Summary of each model component expressed in terms of regression coefficients. Panel (a) reports the contribution of the covariates used linearly. The suffix μ and σ denote the mean and standard deviation values computed from the original covariates per slope unit. CAR8d represents the dynamic rainfall covariate obtained over a 8-day cumulative antecedent window. Panels (b), (c) and (d) report the contribution of the nonlinear cases.

CV tests, here we observe a much larger spread of the resulting ROC curves. The situation goes back to an excellent performance for the LOLEO, as shown in Fig. 7b.

4.6. External cross-validation

The availability of inventories in nearby areas of study site, helped to test the model transferability over an independent dataset, for landslide events mapped far away. A total of five external sites are used for such a test, where three of the sites are still located within Vietnam (but in the south) and the other two are located in Laos (see Fig. 8). The resulting AUC values in Fig. 8 are good to excellent with an exception to test site 4, which gives poor but better-than-random predictions.

4.7. Probability threshold

To translate the model into an early warning system, one of the main requirements is to convert the continuous spectrum of probabilities into a dichotomous output that expresses the probabilistic expectation of a SU to be potentially stable or unstable. To binarize the probability spectrum, we initially assessed the True Negative Rate (TNR) and the

True Positive Rate (TPR) at every 0.05th quantile for each of the LOLEO temporal validations. Fig. 9 depicts the patterns of TNR and TPR for each probability cut-off, whose intersection we considered suitable to choose a cutoff. Specifically, we took the six intersection points, and took the mean of the corresponding probabilities as our reference cutoff.

4.8. Web application

The interactive interface of the GEE application visualizes the mean susceptibility and converts them directly into alert levels using the probability cutoff mentioned in the previous section. In the backend, the platform essentially takes the posterior mean of each covariate effect and solves the additive equation obtained from the original fitted model but over the data obtained for any date selected by the user. Notably, this web-App was built as a proof-of-concept and cannot be used for predictive purposes because CHIRPS products become available in GEE only after approximately six weeks. In other words, our web-App can be used to visualize previous events but cannot be used as a forecasting tool yet, given the unavailability of CHIRPS forecast product (Harrison et al., 2022) in GEE to integrate in the webApp. The webApp can be accessed at this link: <https://mahnoorahmed5593.users.earthengine.app/view/dy>

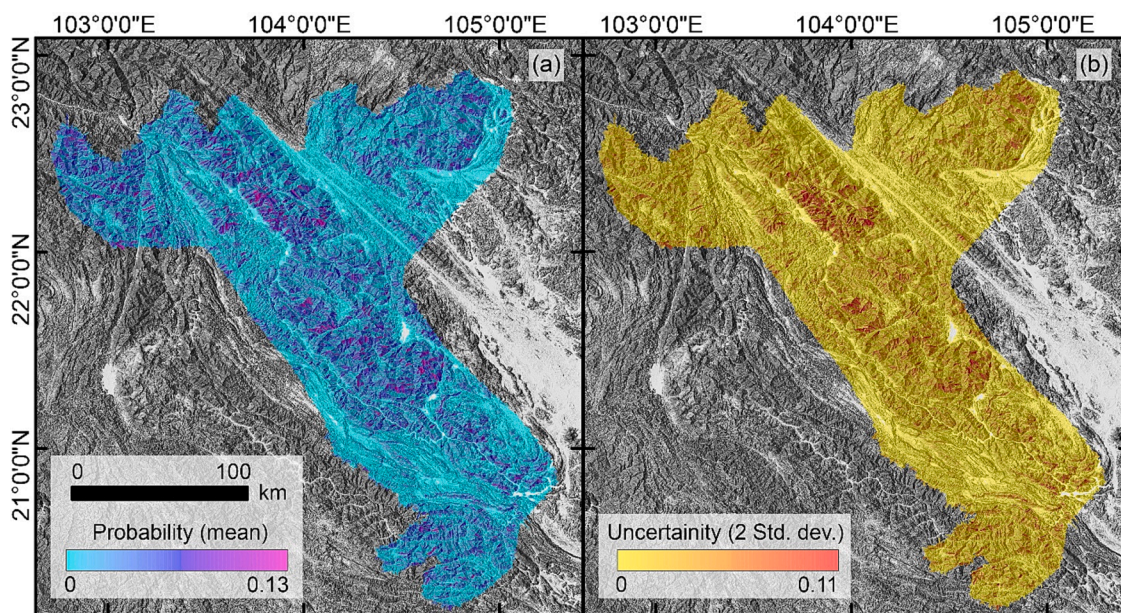


Fig. 4. Combined susceptibility of six inventories (used in calibration). Panel (a) showing the mean susceptibility, panel (b) showing the 95% credible interval.

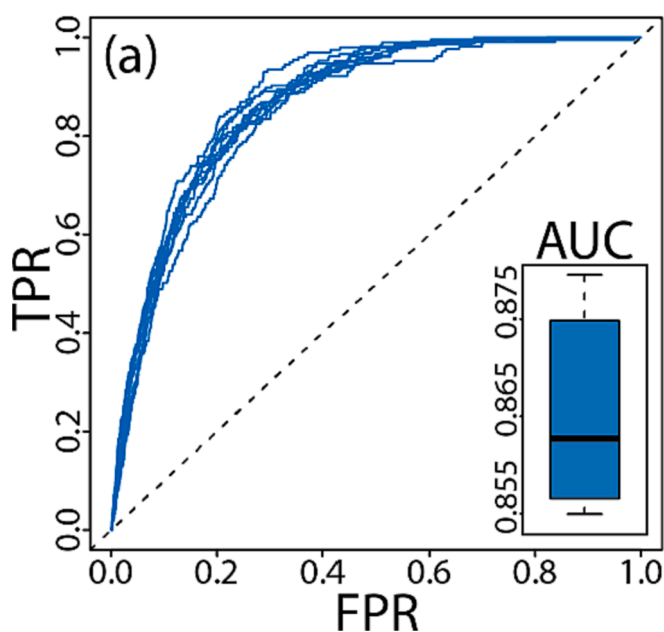


Fig. 5. ROC curves for AUC retrieved in 10-fold cross validation scheme along with the expanding range of AUC values.

namicsusceptibility.

5. Discussion

Starting with the model selection tool, the results indicate the most suitable rainfall-window for our study area to be eight days. Theoretically, a very short window would be indicative of the effect of intense rainfall discharge associated to short cloudburst. However, the emerging 8-days aggregation window is diagnostic of a system where the duration also plays a determinant role.

Most of the literature dedicated to temporal landslide prediction is based on rainfall thresholds and only very few recent studies have framed the same in the multivariate space-time data-driven contexts (see Nocentini et al., 2023; Steger et al., 2023). In this work, we follow

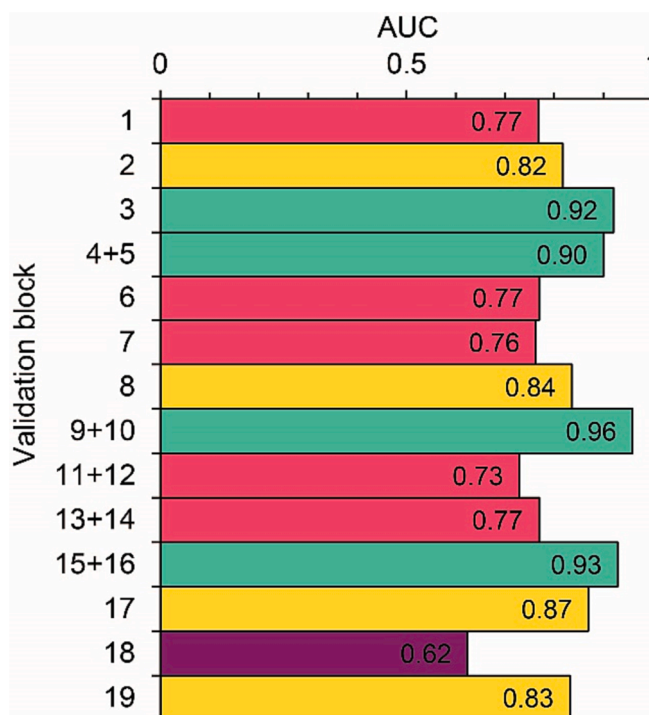


Fig. 6. AUC values for corresponding grid cells and combinations of grid cells obtained from the lattice over the study area for spatial validation. Purple: low AUC, Red: acceptable AUC, Yellow: good AUC, Green: excellent AUC. (For interpretation of the references to colour in this figure legend, the reader is referred to the web version of this article.)

an analogous approach, leaning towards a probabilistic solution that holistically integrates the rainfall signal together with terrain characteristics.

Another interesting element we explore here relates to the use of suitable model assessment tools. In fact, space-time models can exhibit an internal spatio-temporal dependence, that often leads to overly positive performance. For this reason, CV routines should break up any residual dependence in the data, in order to highlight how a model

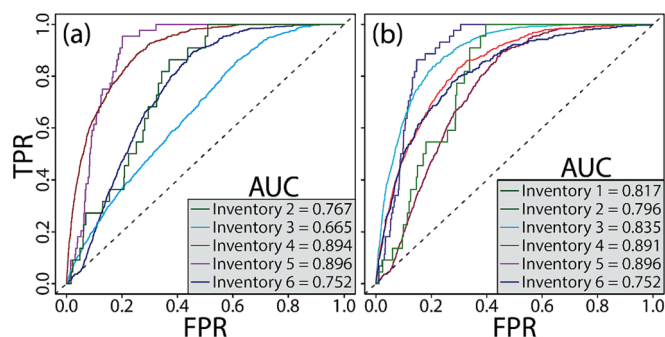


Fig. 7. ROC curves with AUC for panel (a) showing sequential temporal validation and panel (b) showing LOLEO temporal validation.

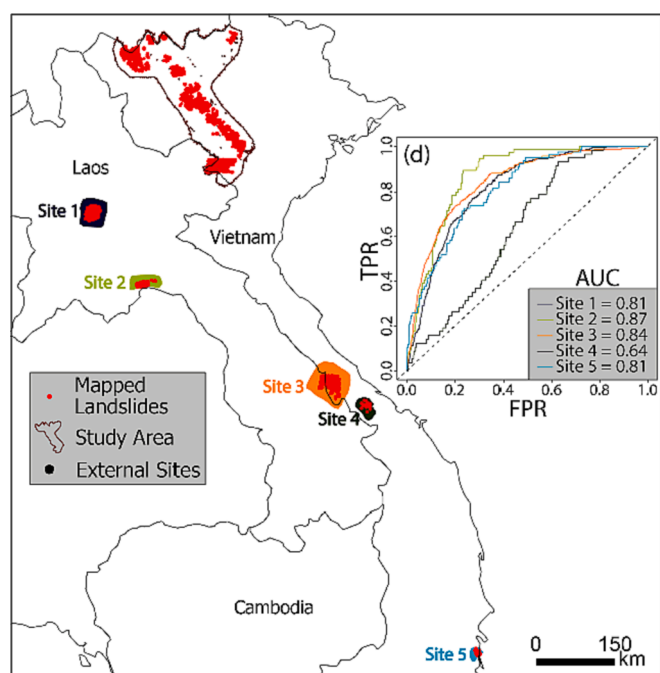


Fig. 8. External validation sites and their respective AUC values in external cross-validation scheme.

actually predicts over unseen test data. In this work, we do this extensively, exploring a number of spatial and temporal CV routines.

The importance of such tools inevitably falls on how efficiently a given data-driven model can be extended towards its operational use. In fact, operational LEWS are often subject to large false positives. These are due to overestimation of the landslide occurrence probability in areas that are stable. Our model, irrespectively of the CV at hand, showed very high prediction capacity, which in turn suggests that the inclusion of terrain attributes into the model helps with suitably classifying the landscape. Similar considerations can be made for false negatives cases, which usually refer to problematic situations where the failure of a given LEWS potentially leads to casualties. Precisely for this reason, we prescribe extensive validation tests, something that in this work have displayed not only locations and times where the model successfully performed but also where and when it failed. Specifically, the SCV highlighted the southernmost sector of the study area (grid 18, see Fig. 2) to be associated with the least classification performance (Fig. 6). Interestingly, when we extended the SCV outside the boundaries of the study area through the external validation test, moving further to the south and west, it did not show a consistent performance drop. Actually, most of the unstable SUs were successfully predicted with the exception of site 4 (see Fig. 8). Therefore, since our model does

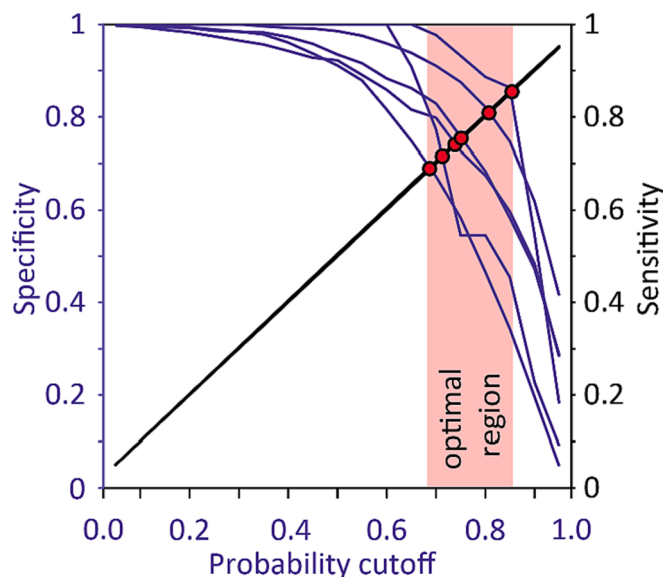


Fig. 9. Combination of six inventories (when each used for validation) displaying sensitivity and specificity at every 0.05th quantile for selecting a threshold to define a probabilistic cutoff.

not include some important covariate information (lithology, distance to road and river, etc.), which can be used to enhance the model and prediction ability, we cannot definitively conclude the reason behind this specific performance drop. Irrespective of such site-specific results, our space-time model suitably predicted the distribution of stable/unstable SUs. However, the assessment discussed so far mainly revolves around the spatial dimension and needs to be therefore extended in time for our model to be evaluated as a LEWS valid alternative. We explored this element in our sequential and LOLEO-CV procedures, where almost all out-of-sample results were associated to an excellent performance. The only exception corresponded to the output of validating on inventory 2 in the sequential temporal validation scheme (see Fig. 7a) which interestingly is associated with the least number of landslides among all. Therefore, the low performance shown in this case leads to two considerations. The first one is that the reason for such drop can be justified with a model that may have locally overestimated the slope response. In turn, this implies that a potential failure if adopted as a LEWS would most likely produce false positives, and would therefore not lead to expected losses, which are common in case of the opposite error type. Also, a possible reason for the performance drop may be due to the error in the dating corresponding to a possible window of five days (see Table 2). This is something that unfortunately cannot be addressed here but that future research directions could potentially solve. In fact, a number of recent studies are trying to limit the error in landslide dating by incorporating information (coherence amplitude drop) from radar satellites in addition to the traditional optical one. Moreover, an increasing number of investments in new constellations would likely cover the earth surface on a more frequent basis in the future, thus limiting the dating error even further.

We also stress once more the importance of an uncertainty estimation to be incorporated as part of any probabilistic model for landslide prediction. Here this is possible to produce it natively due to our Bayesian framework, but we also recommend it in case of frequentist alternatives through bootstrapping. Unfortunately, this is not always part of LEWS.

As an additional nested experiment, we also tested the most suitable probability cutoff representative of multiple available landslide inventories. To do so, we have proposed a combination of sensitivity and specificity values to be explored as a function of a quantile description of the susceptibility spectrum (optimal region roughly between the 0.70th

–0.85th quantiles). The resulting cutoff was used to maximize the classification results displayed through the LEWS, which we translated into the ‘warning’ and ‘no warning’ shown in our interactive GEE WebApp. Notably, our WebApp highlights both the strengths of our approach as well as its weaknesses. In fact, as interesting as our space–time model may be and as transparent our results may be through the WebApp, the system is bound to the rainfall product we used (CHIRPS). This product has a native latency of 1.5 months, which is the time required to make the data available in GEE, after the data itself have been re-processed to minimize the bias between raw radar acquisitions and ground-based rain gauge measures. For this reason, our model is only theoretically useful in an operational sense. In reality, by the time the rainfall estimates become available, potential landslides have already manifested and produced damages. Currently, we see our model as a proof-of-concept of how the future generation of LEWS may become. However, for this to happen, we already see potential improvements in the form of rainfall data usage and processing. The first development involves the use of rainfall forecasts (e.g., GPM/TRMM) rather than re-processed data. In fact, if a LEWS would prove to suitably predict landslides as a function of past records of precipitation forecast, one could then use the space–time architecture as the basis for simulating future unstable SUs, plugging in future rainfall projections. However, even in this case, two main issues may affect the rainfall data and hence the model itself. The former is the difference between forecast data and rain gauge measurements, which should be ideally minimized. Interestingly, a number of valid solutions have been recently shown to minimize the gap or bias between observations and satellite estimates, individually (Beck et al., 2019, 2017) or through smart-data blending (Beikahmadi et al., 2023). Therefore, we expect better rainfall products in the future and through them, even better LEWS (Fang et al., 2023a, b). Where we see the major challenge is in the way to account for precipitation uncertainties. Currently, the uncertainty in the expected weather systems varies as one gets closer to the day of interest. In other words, precipitation patterns and amounts forecasted 10 days in advance may be different and less reliable as compared to the same parameters forecasted a day or just few hours ahead of time (Cuo et al., 2011). Our current regional model requires 8-days cumulative antecedent rainfall, but other study areas may require less. Therefore, the potential transferability of such space–time solution would need to be tested also in the context of different uncertainty levels in the rainfall input. In this sense, we see the Bayesian framework as a perfect modeling platform to propagate different levels of uncertainty, recommending it especially in such cases, and among the available solutions, INLA would most likely offer the best estimation paradigm that allows fast Bayesian inference with relatively complex models (Simpson et al., 2011).

Ultimately, we should stress that our model is currently valid only at the scale of the northern sector of Vietnam. As is, it is potentially transferrable in neighboring regions, especially with analogous terrain characteristics and exposed to analogous meteorological stresses. However, such experiments have not been made part of the present contribution. Thanks to the availability of landslides across other sectors of the Lower Mekong Region, we are now in the process of testing an extension of the model presented here but trained over the whole area where Amatya et al. (2022) mapped landslides. In the future, we plan to compare the performances of the two models, highlighting differences when a regional model such as the present one is benchmarked against a near continental one, and vice-versa.

6. Conclusion

Early warning systems for rainfall-induced landslides have historically treated the precipitation signal separately from the landscape characteristics typical of susceptibility studies. However, space–time data-driven solutions allow one for incorporating both elements at once, potentially opening up for a new generation of alert systems. This work explores this topic, using several landslide inventories mapped for the

northern territory of Vietnam. In doing so, we demonstrate how space–time statistics can efficiently predict landslide occurrences, featuring a number of nested experiments, from the use of Bayesian models, to performance assessment via a suite of spatiotemporal CVs and ultimately by showcasing how web applications can graphically convert the results in a way that anyone can freely access them.

Despite the novelty, a few elements still require further investigation before offering operational solutions, among them the use of rainfall forecast data rather than past projections. Moreover, we also envision additional efforts to be required for moving beyond the susceptibility context. For instance, one could model the extent of the landslides in space and time to ultimately generate space–time intensities rather than occurrence probabilities (Lombardo et al., 2020, 2018). Ultimately, this approach could even be extended to bind exposure data in space and time, giving birth to risk-oriented LEWS. To do so, one would need the statistic information of buildings and infrastructure as well as the dynamic information of population densities. Overall, this is to say that space–time data-driven models are at an infancy phase in the context of landslides. They can certainly constitute the foundation for even systems that may exploit reliable rainfall forecast and return impact-based predictions.

CRediT authorship contribution statement

Mahnoor Ahmed: . **Hakan Tanyas:** . **Raphaël Huser:** . **Ashok Dahal:** . **Giacomo Titti:** . **Lisa Borgatti:** Writing – review & editing. **Mirko Francioni:** Writing – review & editing. **Luigi Lombardo:** .

Declaration of competing interest

The authors declare that they have no known competing financial interests or personal relationships that could have appeared to influence the work reported in this paper.

Data availability

Data and codes are attached as [supplementary material](#)

Appendix A. Supplementary material

Supplementary data to this article can be found online at <https://doi.org/10.1016/j.jag.2023.103593>.

References

- Adler, R.F., Huffman, G.J., Chang, A., Ferraro, R., Xie, P.P., Janowiak, J., Rudolf, B., Schneider, U., Curtis, S., Bolvin, D., Gruber, A., Susskind, J., Arkin, P., Nelkin, E., 2003. The version-2 global precipitation climatology project (GPCP) monthly precipitation analysis (1979–present). *J. Hydrometeorol.* 4, 1147–1167. [https://doi.org/10.1175/1525-7541\(2003\)004<1147:TVGPCP>2.0.CO;2](https://doi.org/10.1175/1525-7541(2003)004<1147:TVGPCP>2.0.CO;2).
- Al-Thuwaynee, O.F., Melillo, M., Gariano, S.L., Park, H.J., Kim, S.-W., Lombardo, L., Hader, P., Mohajane, M., Quevedo, R.P., Catani, F., Aydda, A., 2023. DEWS: A QGIS tool pack for the automatic selection of reference rain gauges for landslide-triggering rainfall thresholds. *Environ. Model. Softw.* 162, 105657. <https://doi.org/10.1016/j.envsoft.2023.105657>.
- Alvioli, M., Marchesini, I., Reichenbach, P., Rossi, M., Ardizzone, F., Fiorucci, F., Guzzetti, F., 2016. Automatic delineation of geomorphological slope units with r. slopeunits v1.0 and their optimization for landslide susceptibility modeling. *Geosci. Model Dev.* 9, 3975–3991. <https://doi.org/10.5194/GMD-9-3975-2016>.
- Amatya, P., Kirschbaum, D., Stanley, T., 2022. Rainfall-induced landslide inventories for Lower Mekong based on Planet imagery and a semi-automatic mapping method. *Geosci. Data J.* 00, 1–13. <https://doi.org/10.1002/gdj3.145>.
- Bakka, H., Rue, H., Fuglstad, G.A., Riebler, A., Bolin, D., Illian, J., Krainski, E., Simpson, D., Lindgren, F., 2018. Spatial modeling with R-INLA: A review. *Wiley Interdiscip. Rev. Comput. Stat.* 10, e1443.
- Bangalore, M., Smith, A., Veldkamp, T., 2019. Exposure to Floods, Climate Change, and Poverty in Vietnam. *Econ. Disasters Clim. Change* 3, 79–99. <https://doi.org/10.1007/S41885-018-0035-4>.
- Beck, H.E., Vergopolan, N., Pan, M., Levizzani, V., Dijk, A.I.J.M.V., Weedon, G.P., Brocca, L., Pappenberger, F., Huffman, G.J., Wood, E.F., 2017. Global-scale evaluation of 22 precipitation datasets using gauge observations and hydrological

- modeling. *Hydrol. Earth Syst. Sci.* 21, 6201–6217. <https://doi.org/10.5194/HESS-21-6201-2017>.
- Beck, H.E., Wood, E.F., Pan, M., Fisher, C.K., Miralles, D.G., Dijk, A.I.J.M.V., McVicar, T.R., Adler, R.F., 2019. MSWEP V2 Global 3-Hourly 0.1° Precipitation: Methodology and Quantitative Assessment. *Bull. Am. Meteorol. Soc.* 100, 473–500. <https://doi.org/10.1175/BAMS-D-17-0138.1>.
- Beikahmadi, N., Francipane, A., Noto, L.V., 2023. Smart Data Blending Framework to Enhance Precipitation Estimation through Interconnected Atmospheric, Satellite, and Surface Variables. *Hydrol.* 2023, 10, 128 10, 128. <https://doi.org/10.3390/HYDROLOGY10060128>.
- Biswas, N.K., Stanley, T.A., Kirschbaum, D.B., Amatya, P.M., Meechaiya, C., Poortinga, A., Towashiraporn, P., 2022. A dynamic landslide hazard monitoring framework for the Lower Mekong Region. *Front. Earth Sci.* 10 <https://doi.org/10.3389/FEART.2022.1057796/BIBTEX>.
- Brenning, A., 2005. Spatial prediction models for landslide hazards: review, comparison and evaluation. *Nat. Hazards Earth Syst. Sci.* 5, 853–862. <https://doi.org/10.5194/NHESS-5-853-2005>.
- Brenning, A., 2012. Spatial cross-validation and bootstrap for the assessment of prediction rules in remote sensing: The R package sprrorest. In: *International Geoscience and Remote Sensing Symposium (IGARSS)*. IEEE, pp. 5372–5375. <https://doi.org/10.1109/IGARSS.2012.6352393>.
- Budimir, M.E.A., Atkinson, P.M., Lewis, H.G., 2015. A systematic review of landslide probability mapping using logistic regression. *Landslides* 12, 419–436. <https://doi.org/10.1007/S10346-014-0550-5/FIGURES/9>.
- Bui, D.T., Lofman, O., Revhaug, I., Dick, O., 2011. Landslide susceptibility analysis in the Hoa Binh province of Vietnam using statistical index and logistic regression. *Nat. Hazards* 59, 1413–1444. <https://doi.org/10.1007/s11069-011-9844-2>.
- Bui, D.T., Pradhan, B., Lofman, O., Revhaug, I., Dick, O.B., 2012. Spatial prediction of landslide hazards in Hoa Binh province (Vietnam): A comparative assessment of the efficacy of evidential belief functions and fuzzy logic models. *CATENA* 96, 28–40. <https://doi.org/10.1016/J.CATENA.2012.04.001>.
- Bui, D.T., Pradhan, B., Lofman, O., Revhaug, I., Dick, Ø.B., 2013. Regional prediction of landslide hazard using probability analysis of intense rainfall in the Hoa Binh province. *Nat. Hazards* 66, 707–730. <https://doi.org/10.1007/S11069-012-0510-0/FIGURES/12>.
- Carrara, A., Cardinali, M., Detti, R., Guzzetti, F., Pasqui, V., Reichenbach, P., 1991. GIS techniques and statistical models in evaluating landslide hazard. *Earth Surf. Process. Landf.* 16, 427–445. <https://doi.org/10.1002/ESP.3290160505>.
- Chauhan, S., Sharma, M., Arora, M.K., Gupta, N.K., 2010. Landslide Susceptibility Zonation through ratings derived from Artificial Neural Network. *Int. J. Appl. Earth Obs. Geoinformation* 12, 340–350. <https://doi.org/10.1016/j.jag.2010.04.006>.
- Chikalomo, E.E., Mavrouli, O.C., Ettema, J., van Westen, C.J., Muntohar, A.S., Mustofa, A., 2020. Satellite-derived rainfall thresholds for landslide early warning in Bogowonto Catchment, Central Java, Indonesia. *Int. J. Appl. Earth Obs. Geoinformation* 89, 102093. <https://doi.org/10.1016/j.jag.2020.102093>.
- Chung, C.J.F., Fabbri, A.G., 2003. Validation of Spatial Prediction Models for Landslide Hazard Mapping. *Nat. Hazards* 30, 451–472. <https://doi.org/10.1023/B:NHAZ.0000007172.62651.2B>.
- Chung, C.-J., Fabbri, A.G., 2008. Predicting landslides for risk analysis — Spatial models tested by a cross-validation technique. *Geomorphology* 94, 438–452. <https://doi.org/10.1016/j.geomorph.2006.12.036>.
- Cuo, L., Pagano, T.C., Wang, Q.J., 2011. A Review of Quantitative Precipitation Forecasts and Their Use in Short- to Medium-Range Streamflow Forecasting. *J. Hydrometeorol.* 12, 713–728. <https://doi.org/10.1175/2011JHM1347.1>.
- Didan, K., 2015. MYD13Q1 MODIS/Aqua Vegetation Indices 16-Day L3 Global 250m SIN Grid V006. <https://doi.org/10.5067/MODIS/MYD13Q1.006>.
- Epifanio, B., Zézere, J.L., Neves, M., 2014. Susceptibility assessment to different types of landslides in the coastal cliffs of Lourinhã (Central Portugal). *J. Sea Res.* 93, 150–159. <https://doi.org/10.1016/j.seares.2014.04.006>.
- Fang, Z., Wang, Y., van Westen, C., Lombardo, L., 2023a. Space-Time Landslide Susceptibility Modeling Based on Data-Driven Methods. *Mathem. Geosci.* 1–20.
- Fang, Z., Tanyas, H., Gorum, T., Dahal, A., Wang, Y.i., Lombardo, L., 2023b. Speech-recognition in landslide predictive modelling: A case for a next generation early warning system. *Environ. Modell. Softw.* 170, 105833.
- Funk, C., Peterson, P., Landsfeld, M., Pedreros, D., Verdin, J., Shukla, S., Husak, G., Rowland, J., Harrison, L., Hoell, A., Michaelsen, J., 2015. The climate hazards infrared precipitation with stations—a new environmental record for monitoring extremes. *Sci. Data* 2, <https://doi.org/10.1038/sdata.2015.66>.
- Gariano, S.L., Rianna, G., Petrucci, O., Guzzetti, F., 2017. Assessing future changes in the occurrence of rainfall-induced landslides at a regional scale. *Sci. Total Environ.* 596–597, 417–426. <https://doi.org/10.1016/j.scitotenv.2017.03.103>.
- Gian, Q.A., Tran, D.T., Nguyen, D.C., Nhu, V.H., Bui, D.T., 2017. Design and implementation of site-specific rainfall-induced landslide early warning and monitoring system: a case study at Nam Dan landslide (Vietnam). *Geomat. Nat. Hazards Risk* 8, 1978–1996. <https://doi.org/10.1080/19475705.2017.1401561>.
- Goetz, J.N., Brenning, A., Petschko, H., Leopold, P., 2015. Evaluating machine learning and statistical prediction techniques for landslide susceptibility modeling. *Comput. Geosci.* 81, 1–11. <https://doi.org/10.1016/j.cageo.2015.04.007>.
- Gorelick, N., Hancher, M., Dixon, M., Ilyushchenko, S., Thau, D., Moore, R., 2017. Google Earth Engine: Planetary-scale geospatial analysis for everyone. *Remote Sens. Environ.* 202, 18–27. <https://doi.org/10.1016/j.rse.2017.06.031>.
- Görüm, T., 2019. Tectonic, topographic and rock-type influences on large landslides at the northern margin of the Anatolian Plateau. *Landslides* 16, 333–346. <https://doi.org/10.1007/S10346-018-1097-7>.
- Guzzetti, F., Reichenbach, P., Ardizzone, F., Cardinali, M., Galli, M., 2006. Estimating the quality of landslide susceptibility models. *Geomorphology* 81, 166–184. <https://doi.org/10.1016/j.geomorph.2006.04.007>.
- Guzzetti, F., Peruccacci, S., Rossi, M., Stark, C.P., 2007. Rainfall thresholds for the initiation of landslides in central and southern Europe. *Meteorol. Atmospheric Phys.* 98, 239–267. <https://doi.org/10.1007/s00703-007-0262-7>.
- Guzzetti, F., Peruccacci, S., Rossi, M., Stark, C.P., 2008. The rainfall intensity-duration control of shallow landslides and debris flows: An update. *Landslides* 5, 3–17. <https://doi.org/10.1007/s10346-007-0112-1>.
- Guzzetti, F., Gariano, S.L., Peruccacci, S., Brunetti, M.T., Marchesini, I., Rossi, M., Melillo, M., 2020. Geographical landslide early warning systems. *Earth-Sci. Rev.* 200, 102973. <https://doi.org/10.1016/J.EARSCIREV.2019.102973>.
- Ha, N.D., Sayama, T., Sassa, K., Takara, K., Uzuoka, R., Dang, K., Pham, T.V., 2020. A coupled hydrological-geotechnical framework for forecasting shallow landslide hazard—a case study in Halong City, Vietnam. *Landslides* 17, 1619–1634. <https://doi.org/10.1007/S10346-020-01385-8/FIGURES/15>.
- Harrison, L., Landsfeld, M., Husak, G., Davenport, F., Shukla, S., Turner, W., Peterson, P., Funk, C., 2022. Advancing early warning capabilities with CHIRPS-compatible NCEP GEFS precipitation forecasts. *Sci. Data* 9, 1–13. <https://doi.org/10.1038/s41597-022-01468-2>.
- Hastie, T.J., 2017. *Generalized Additive Models*, 1st ed, Statistical Models in S. Routledge. <https://doi.org/10.1201/9780203738535-7>.
- He, Y., Zhao, Z., Yang, W., Yan, H., Wenhui, W., Yao, S., Zhang, L., Liu, T., 2021. A unified network of information considering superimposed landslide factors sequence and pixel spatial neighbourhood for landslide susceptibility mapping. *Int. J. Appl. Earth Obs. Geoinformation* 104, 102508. <https://doi.org/10.1016/j.jag.2021.102508>.
- Hidayat, R., Sutanto, S.J., Hidayah, A., Ridwan, B., Mulyana, A., 2019. Development of a landslide early warning system in Indonesia. *Geosci. Switz.* 9 (10), 451.
- Hong, Y., Adler, R., Huffman, G., 2006. Evaluation of the potential of NASA multi-satellite precipitation analysis in global landslide hazard assessment. *Geophys. Res. Lett.* 33 <https://doi.org/10.1029/2006GL028010>.
- Hong, Y., Adler, R.F., 2007. Towards an early-warning system for global landslides triggered by rainfall and earthquake. *Int. J. Remote Sens.* 28, 3713–3719. <https://doi.org/10.1080/01431160701311242>.
- Hosmer, D.W., Lemeshow, S., Sturdivant, R.X., 2003. *Applied Logistic Regression*, Third ed, Wiley Series in Probability and Statistics. John Wiley and Sons Inc. <https://doi.org/10.2307/2532419>.
- Kirschbaum, D.B., Adler, R., Hong, Y., Lerner-Lam, A., 2009. Evaluation of a preliminary satellite-based landslide hazard algorithm using global landslide inventories. *Nat. Hazards Earth Syst. Sci.* 9, 673–686. <https://doi.org/10.5194/nhess-9-673-2009>.
- Kirschbaum, D.B., Adler, R., Hong, Y., Kumar, S., Peters-Lidard, C., Lerner-Lam, A., 2012. Advances in landslide nowcasting: Evaluation of a global and regional modeling approach. *Environ. Earth Sci.* 66, 1683–1696. <https://doi.org/10.1007/s12665-011-0990-3>.
- Kirschbaum, D., Stanley, T., 2018. Satellite-Based Assessment of Rainfall-Triggered Landslide Hazard for Situational Awareness. *Earths Future* 6, 505–523. <https://doi.org/10.1002/2017EF000715>.
- Lee, C.T., Huang, C.C., Lee, J.F., Pan, K.L., Lin, M.L., Dong, J.J., 2008. Statistical approach to storm event-induced landslides susceptibility. *Nat. Hazards Earth Syst. Sci.* 8, 941–960. <https://doi.org/10.5194/NHESS-8-941-2008>.
- Leempoel, K., Parisod, C., Geiser, C., Dapra, L., Vittoz, P., Joost, S., Kriticos, D., 2015. Very high-resolution digital elevation models: Are multi-scale derived variables ecologically relevant? *Methods Ecol. Evol.* 6 (12), 1373–1383.
- Lin, Q., Lima, P., Steger, S., Glade, T., Jiang, T., Zhang, J., Liu, T., Wang, Y., 2021. National-scale data-driven rainfall induced landslide susceptibility mapping for China by accounting for incomplete landslide data. *Geosci. Front.* 12 (6), 101248. <https://doi.org/10.1016/J.GSF.2021.101248>.
- Lombardo, L., Opitz, T., Huser, R., 2018. Point process-based modeling of multiple debris flow landslides using INLA: an application to the 2009 Messina disaster. *Stoch. Environ. Res. Risk Assess.* 32, 2179–2198. <https://doi.org/10.1007/S00477-018-1518-0/TABLES/5>.
- Lombardo, L., Opitz, T., Ardizzone, F., Guzzetti, F., Huser, R., 2020. Space-time landslide predictive modelling. *Earth-Sci. Rev.* 209, 103318. <https://doi.org/10.1016/j.earscirev.2020.103318>.
- Lombardo, L., Tanyas, H., 2020. Chrono-validation of near-real-time landslide susceptibility models via plug-in statistical simulations. *Eng. Geol.* 278, 105818. <https://doi.org/10.1016/J.ENGCEO.2020.105818>.
- Mutanga, O., Kumar, L., 2019. Google Earth Engine Applications. *Remote Sens.* 11 (5), 591. <https://doi.org/10.3390/RS11050591>.
- Naidu, S., Sajinkumar, K.S., Oommen, T., Anuja, V.J., Samuel, R.A., Muraleedharan, C., 2018. Early warning system for shallow landslides using rainfall threshold and slope stability analysis. *Geosci. Front. Reliability Anal. Geotechn. Infrastruct.* 9, 1871–1882. <https://doi.org/10.1016/j.gsf.2017.10.008>.
- Neteler, M., Mitasova, H., 2013. *Open source GIS: a GRASS GIS approach*. Springer Science & Business Media.
- Neuhäuser, B., Damm, B., Terhorst, B., 2012. GIS-based assessment of landslide susceptibility on the base of the Weights-of-Evidence method. *Landslides* 9, 511–528. <https://doi.org/10.1007/S10346-011-0305-5>.
- Nguyen, K.C., Katzfey, J.J., McGregor, J.L., 2014. Downscaling over Vietnam using the stretched-grid CCAM: Verification of the mean and interannual variability of rainfall. *Clim. Dyn.* 43, 861–879. <https://doi.org/10.1007/S00382-013-1976-5>.
- Nocentini, N., Rosi, A., Segoni, S., Fanti, R., 2023. Towards landslide space-time forecasting through machine learning: the influence of rainfall parameters and model setting. *Front. Earth Sci.* 11 <https://doi.org/10.3389/FEART.2023.1152130/BIBTEX>.

- Ohlmacher, G.C., 2007. Plan curvature and landslide probability in regions dominated by earth flows and earth slides. *Eng. Geol.* 91, 117–134. <https://doi.org/10.1016/J.ENGGEOL.2007.01.005>.
- Petley, D., 2012. Global patterns of loss of life from landslides. *Geology* 40, 927–930. <https://doi.org/10.1130/G33217.1>.
- Qiu, H., Cui, P., Regmi, A.D., Hu, S., Zhang, Y., He, Y., 2018. Landslide distribution and size versus relative relief (Shaanxi Province, China). *Bull. Eng. Geol. Environ.* 77, 1331–1342. <https://doi.org/10.1007/S10064-017-1121-5/TABLES/1>.
- Reichenbach, P., Rossi, M., Malamud, B.D., Mihir, M., Guzzetti, F., 2018. A review of statistically-based landslide susceptibility models. *Earth-Sci. Rev.* 180, 60–91. <https://doi.org/10.1016/J.EARSCIREV.2018.03.001>.
- Remondo, J., González-Díez, A., Terán, J., Cendrero, A., Fabbri, A., Chung, C.-J., 2003. Validation of Landslide Susceptibility Maps; Examples and Applications from a Case Study in Northern Spain. *Nat. Hazards* 30, 437–449. <https://doi.org/10.1023/B:NHAZ.0000007201.80743.fc>.
- RStudio Team, 2023. RStudio: Integrated Development for R.
- Rue, H., Martino, S., Chopin, N., 2009. Approximate Bayesian inference for latent Gaussian models by using integrated nested Laplace approximations. *J. R. Stat. Soc. Ser. B Stat. Methodol.* 71, 319–392. <https://doi.org/10.1111/J.1467-9868.2008.00700.X>.
- Segoni, S., Piciullo, L., Gariano, S.L., 2018. A review of the recent literature on rainfall thresholds for landslide occurrence. *Landslides* 15, 1483–1501. <https://doi.org/10.1007/S10346-018-0966-4>.
- Simpson, D., Lindgren, F., Rue, H., 2011. Fast approximate inference with INLA: the past, the present and the future. *arXiv:1105.2982*.
- Stanley, T.A., Kirschbaum, D.B., Benz, G., Emberson, R.A., Amatya, P.M., Medwedeff, W., Clark, M.K., 2021. Data-Driven Landslide Nowcasting at the Global Scale. *Front. Earth Sci.* 9 <https://doi.org/10.3389/FEART.2021.640043/BIBTEX>.
- Steger, S., Moreno, M., Crespi, A., Zellner, P.J., Gariano, S.L., Brunetti, M.T., Melillo, M., Peruccacci, S., Marra, F., Kohrs, R., Goetz, J., Mair, V., Pittore, M., 2023. Deciphering seasonal effects of triggering and preparatory precipitation for improved shallow landslide prediction using generalized additive mixed models. *Nat. Hazards Earth Syst. Sci.* 23, 1483–1506. <https://doi.org/10.5194/NHESS-23-1483-2023>.
- Tang, G., Clark, M.P., Papalexioiu, S.M., Ma, Z., Hong, Y., 2020. Have satellite precipitation products improved over last two decades? A comprehensive comparison of GPM IMERG with nine satellite and reanalysis datasets. *Remote Sens. Environ.* 240, 111697. <https://doi.org/10.1016/J.RSE.2020.111697>.
- Titti, G., van Westen, C., Borgatti, L., Pasuto, A., Lombardo, L., 2021. When Enough Is Really Enough? On the Minimum Number of Landslides to Build Reliable Susceptibility Models. *Geosciences* 11, 469. <https://doi.org/10.3390/GEOSCIENCES11110469>.
- Titti, G., Napoli, G.N., Conoscenti, C., Lombardo, L., 2022. Cloud-based interactive susceptibility modeling of gully erosion in Google Earth Engine. *Int. J. Appl. Earth Obs. Geoinformation* 115, 103089. <https://doi.org/10.1016/J.JAG.2022.103089>.
- Wang, N., Lombardo, L., Gariano, S.L., Cheng, W., Liu, C., Xiong, J., Wang, R., 2021. Using satellite rainfall products to assess the triggering conditions for hydro-morphological processes in different geomorphological settings in China. *Int. J. Appl. Earth Obs. Geoinformation* 102, 102350. <https://doi.org/10.1016/J.JAG.2021.102350>.
- Whalen, A., Hoppitt, W.J.E., 2016. Bayesian model selection with Network Based Diffusion Analysis. *Front. Psychol.* 7 <https://doi.org/10.3389/FPSYG.2016.00409/BIBTEX>.
- Wu, W., Sidle, R.C., 1995. A Distributed Slope Stability Model for Steep Forested Basins. *Water Resour. Res.* 31, 2097–2110. <https://doi.org/10.1029/95WR01136>.
- Yang, S., Berdine, G., 2017. The receiver operating characteristic (ROC) curve. *Southwest Respir. Crit. Care Chron.* 5 <https://doi.org/10.12746/SWRCCC.V5I19.391>.
- Yang, L., Meng, X., Zhang, X., 2011. SRTM DEM and its application advances. *Int. J. Remote Sens.* 32, 3875–3896. <https://doi.org/10.1080/01431161003786016>.
- Zou, K.H., O'Malley, A.J., Mauri, L., 2007. Receiver-operating characteristic analysis for evaluating diagnostic tests and predictive models. *Circulation* 115, 654–657. <https://doi.org/10.1161/CIRCULATIONAHA.105.594929>.